1
Introduction and General Survey of Metal–Metal Bonds

John E. McGrady

1.1
Introduction

The interactions between metal ions continue to challenge our understanding of the nature of the chemical bond. The first decade of the new millennium has been a particularly productive period, with a number of landmark discoveries including the ultrashort Cr^{I}–Cr^{I} bonds [1], the Mg^{I}–Mg^{I} and Zn^{I}–Zn^{I} dimers of Jones [2] and Carmona [3], respectively, and the distannynes [4] and diplumbynes [5], the heavier analogs of acetylene. Moreover, metal–metal bonded systems are increasingly finding applications in fields as diverse as molecular electronics [6], organometallic catalysis [7], and even in enzyme-mediated transformations [8]. The pioneering work in the field dates back almost exactly half a century and is inevitably associated with Cotton and the quadruple bond in $[Re_2Cl_8]^{2-}$ [9–11]. Since that time, the three transition series have proved the most fertile source of metal–metal bonds, largely because the presence of (n + 1)s, (n + 1)p, and nd orbitals in the valence region offers an unrivaled potential for strong interactions. Nevertheless, the transition metals make up fewer than half of the know "metallic" elements, and metal–metal bonds in discrete molecular systems are becoming increasingly well established for the s-, p-, and even the f-block elements [12].

In general, the formation of bonds between metals is a delicate balancing act: on the one hand the valence orbitals involved must be sufficiently diffuse to afford substantial diatomic overlap, on the other, competitive binding of additional ligands must be avoided. In fact, much of the recent progress in the field has come through the elegant design of sterically encumbered ligands that block access of additional ligands to the metal coordination sphere. The intrinsic strength of the bond between two metals depends on many factors, including the number of available electrons and the radial and angular properties of the valence orbitals involved. The angular properties determine the local symmetry of the overlap between metal-based orbitals: σ, π, δ, the latter being unique to systems with valence orbitals with $l > 1$ (i.e., d or f orbitals, Figure 1.1). While undoubtedly iconic in the context of metal–metal interactions, δ bonding is typically very weak and the components with σ and π symmetry dominate the overall bond strength. The radial properties of the orbitals control many of the important periodic trends: radial distribution functions for the valence orbitals in exemplary s-, p-, d-, and f-block elements (Mg, Sn, Cr, and Eu, respectively) are collected in Figure 1.2. In the main groups, the valence ns and/or np orbitals are generally well extended relative to core orbitals and so the equilibrium geometry affords near-optimal overlap. The more diffuse nature of orbitals with higher principal quantum number then leads to reduced overlap and hence to relatively weaker bonds in the heavier members of the group: the multiple bonds in distannenes and distannynes are classic examples. The inert-pair effect also means that metal–metal bonding in the heavier post transition metals is increasingly dominated by np orbitals, the ns character accumulating in nonbonding lone pairs. In the transition series (exemplified by Cr in Figure 1.2), in contrast, the radial maxima of the valence nd orbitals lie in the same region as those of the filled ns and np core, and so diatomic overlap is intrinsically small. In this case, an increase in principal quantum causes a greater fraction of the

Molecular Metal-Metal Bonds: Compounds, Synthesis, Properties, First Edition.
Edited by Stephen T. Liddle.

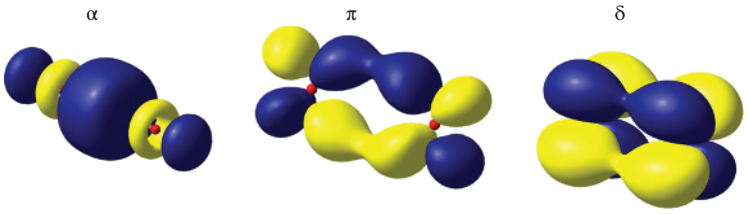

Figure 1.1 σ, π, and δ overlap of d orbitals between two arbitrary metal centers.

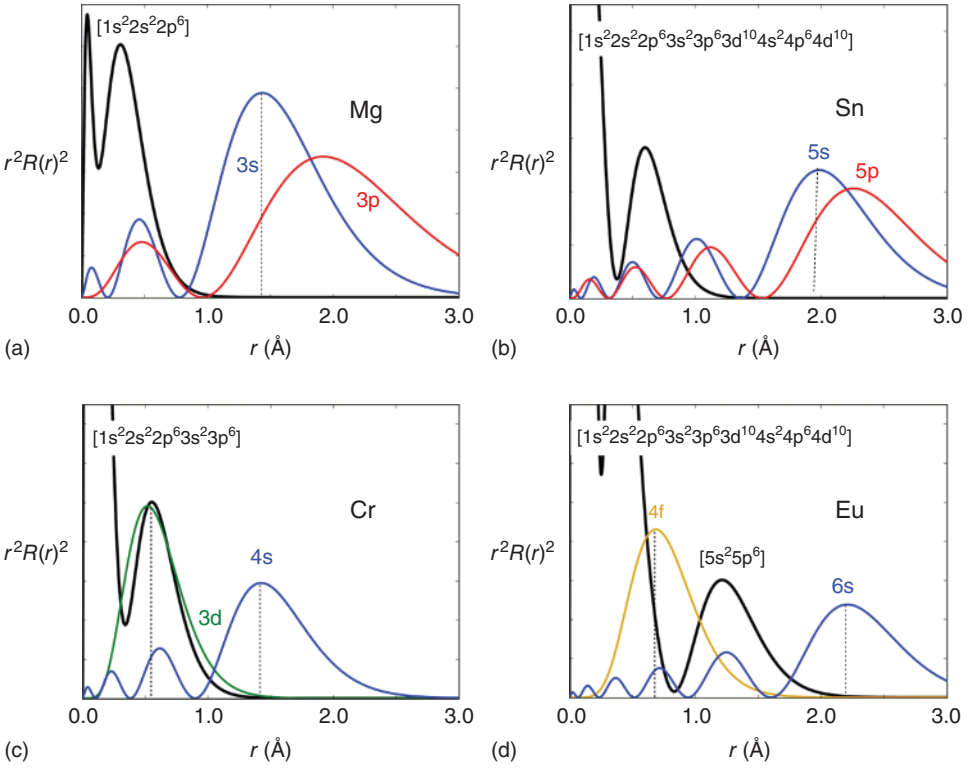

Figure 1.2 Radial distribution functions of the valence orbitals in the (a) s-(Mg), (b) p-(Sn), (c) d-(Cr), and (d) f-(Eu) blocks of the periodic table. Black lines correspond to the core density.

nd orbital to protrude outside the core and so d-d overlap increases, rather than decreases, down a group. The trend in bond strengths is therefore precisely the opposite of that in the main group: metal–metal bonding becomes stronger in the heavier transition metal elements. The lanthanide and actinide series (Eu in Figure 1.2.) can be regarded as extreme versions of the transition elements, with the nf orbitals now lying almost entirely inside the radial maxima of filled (n + 1)s and (n + 1)p and unavailable to participate in effective bonding interactions.

It is important to emphasize from the outset that metal–metal bonds present a substantial challenge to electronic structure theory, particularly where diatomic overlap is weak and the electrons are highly correlated. The chromium dimer, Cr_2, for example, is a notoriously difficult case and has been the subject of debate for decades [13]. Some progress toward a quantitative understanding of these correlation effects has been made through Complete Active Space Self Consistent Field (CASSCF) and related wavefunction-based techniques, but much of our qualitative understanding

of metal–metal bond remains based on single determinant methods. While such methods are necessarily deficient in the limit of weak overlap, they have the considerable advantage of affording a transparent molecular orbital–based picture. Density functional theory (DFT) is the tool of choice in most modern research laboratories, but the early contributions made using Extended Hückel theory, most notably by the Hoffmann school, should be acknowledged [14]. The emphasis in this introduction is firmly on qualitative overlap arguments that have, typically, followed hard on the heels of the synthesis of new types of compound. The coverage reflects the structure of the periodic table, with metal–metal bonds mediated primarily by s orbitals discussed first, followed by the d, f, and p blocks. The purpose of this introductory chapter is to provide a periodic framework for the discussion of specific classes of metal–metal bonds that appear in subsequent chapters.

1.2
Metal–Metal Bonds Involving *s* Orbitals

The chemistry of groups 1 and 2 is characterized almost exclusively by the +1 and +2 oxidation states, respectively, leaving little scope for direct covalent interactions between the metals. Exceptions occur in the relatively electronegative lighter elements, Li and Be, where the occupied bonding orbitals carry substantial metallic character. A textbook case is the electron-deficient Li_4Me_4 tetramer, where the bonding orbitals have both Li–Li and Li–C bonding character and the Li–Li distance is rather short at 2.56 Å [15]. Examples of unsupported metal–metal bonds in subvalent Mg^I species emerged only in the 1980s when species such as HMg–MgH and ClMg–MgCl were characterized in inert matrices [16]. The first species containing direct Mg^I–Mg^I bonds (Mg–Mg = 2.8508(12), 2.8457(8) Å) to be isolated were reported only in 2007 by Jones and Stasch (Figure 1.3) [2]. The Mg–Mg bonding is dominated by the Mg 3s orbital (>90%), with homolytic bond dissociation energies in the region of ~45 kcal mol^{-1}. The radial disparity between the very diffuse 3s valence orbital and a relatively compact [$1s^2 2s^2 2p^6$] core (shown in Figure 1.2) means that the electron density in the bond is somewhat isolated from the nuclei [17–19], and these dimers are very effective two-electron reducing agents [20].

The potential for extending this chemistry to heavier members of group 2 seems rather limited, primarily because the high energy of the ns orbitals makes the interception of the M^I oxidation state increasingly challenging. Moreover, the radial maxima become even more diffuse, making the putative M–M bonds very weak. For example, Ca–Ca bonds have been computed to be almost 1 Å longer than their Mg counterparts, with bond dissociation energies lowered by 50% [21]. On the opposite side of the first transition series in group 12, however, penetration through the nd^{10} core stabilizes the (n + 1)s orbital and contracts its radial maximum, making bonds mediated by the s orbitals accessible once again. Prior to 2004, the chemistry of Zn–Zn bonded species was limited to reports of the Zn_2^{2+} cation in $Zn/ZnCl_2$ melts [22] and the spectroscopic characterization of the dihydride HZn–ZnH in inert matrices [23]. Carmona's report of the structure of dizincocene (Cp*Zn–ZnCp*), with a Zn–Zn separation of 2.3050(3) Å and two parallel Cp* rings, represents the first structurally characterized example of its kind (Figure 1.3) [3]. The nature of the Zn–Zn bond in Zn_2^{2+} and related species had been extensively discussed well before Carmona's seminal discovery [24], but the realization that Cp*Zn–ZnCp* was a stable chemical entity prompted a number of theoretical investigations [25]. Much like the Mg–Mg bond, the Zn–Zn bond in dizincocene is mediated primarily by overlap of the s orbitals (4s in this case), which make up ~90% of the character of the HOMO: symmetry allowed mixing with the p_z and d_{z^2} orbitals is minimal [26]. Compared to the Mg–Mg bonds, however, the contraction of the 4s orbital leads to much shorter and stronger (65 kcal mol^{-1} vs 45 kcal mol^{-1}) bonds. Numerous other Zn–Zn bonded species have emerged in the decade since Carmona's report, primarily with chelating nitrogen-based ligands [27], and these compounds have even found use as reagents in chemical synthesis [28]. The nature of the Zn–Zn bonding appears to be relatively similar

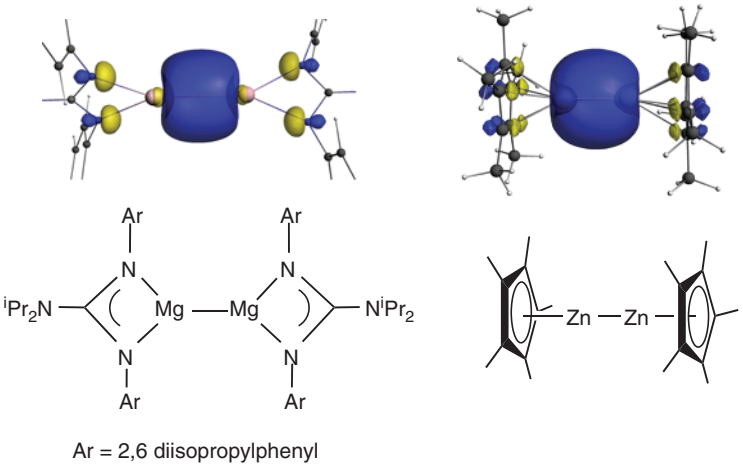

Figure 1.3 HOMOs of ((Ar)NC(N^{i}Pr$_2$)N(Ar))Mg–Mg((Ar)NC(N^{i}Pr$_2$)N(Ar)) and Cp*Zn–ZnCp*.

in all cases, although linear coordination to a strong σ-donor ligand in ArZn–ZnAr (Ar = C_6H_3-2,6-(C_6H_3-2,6-^{i}Pr$_2$)$_2$) [29] results in a somewhat longer Zn–Zn bond (2.3591(9) Å) with more extensive s/p$_z$ mixing, the latter making up ~30% of the Zn character in the HOMO.

The heavier dications Cd_2^{2+} and Hg_2^{2+} are relatively common structural motifs in both the solid state and melts [30], but discrete molecular analogs of the Zn–Zn bonded systems are scarce because coordination of ligands tends to induce disproportionation to M^0 and M^{II}. In fact, the first structurally characterized complex of Hg_2^{2+}, the silyl complex $Hg_2[Si(SiMe_2SiMe_3)_3]_2$ with an Hg–Hg separation of 2.6569(1) Å, was described only in 1999 [31]. Alongside ArZn–ZnAr, the Cd–Cd [32] and Hg–Hg [33] analogue presented the first opportunity to compare trends in bonding down group 12 within an isostructural series. The Cd–Cd bond appears to be rather similar to the Zn–Zn analog, with dominant 5s character mixed with some 5p$_z$. In the mercury congener, however, relativistic stabilization of the 6s orbital reduces the 5d$_{z^2}$/6s separation, and ~5% d$_{z^2}$ character is present in the Hg–Hg bonding HOMO. In conjunction with the lanthanide contraction, the result is that the Hg–Hg bond (2.5738(3) Å) is marginally shorter than its Cd–Cd analog (2.6257(5) Å) despite the presence of 32 extra electrons in the core shells.

The predominance of the +3 oxidation state in aluminum chemistry means that, like the group 1, 2, and 12 analogs, homometallic covalent Al–Al bonds are relatively scarce. A number of subvalent Al^I and Al^{II} species have, however, been synthesized, including the first molecular Al–Al bond in $Al_2(CH(SiMe_3)_2)_4$ (Al–Al = 2.660(1) Å) [34]. Even lower oxidation states of Al are generally stabilized through the formation of pseudo-spherical clusters such as the tetrahedral Al^I species, $Cp^*_4Al_4$ [35] and the remarkable icosahedral "superhalide" ion, $[Al_{13}]^-$ [36]. The latter is observed in gas-phase experiments, where it is notably resistant to reaction with oxygen compared to neighboring members of the $[Al_n]^-$ series. The stability of the $[Al_{13}]^-$ cluster can be understood using a delocalized "jellium" model, where the 40 valence electrons are confined in an approximately spherical positive potential generated by the nuclei and the core 1s, 2s and 2p electrons (Figure 1.4). The degeneracies in the energy level ordering shown in Figure 1.4 ($1a_{1g} < 1t_{1u} < 1h_g < 2a_{1g} < 2t_{1u} < 1g_u = 1t_{2u} < 2h_g$) are reminiscent of a superatomic ordering sequence 1s < 1p < 1d < 2s < 2p < 1f < 2d, reflecting the approximate spherical symmetry of the confining potential.

In contrast to the now relatively extensive metal–metal bonded chemistry of subvalent Mg, Al, and Zn, homometallic bonds involving the 6s and 7s orbitals of the lanthanide and actinides elements are rare (diatomic overlap between the 5f orbitals in U_2 and other cases is discussed later). Their absence is largely a consequence of the relatively low second and third ionization energies (compared to Al), which reduce the stability of the +1 and +2 oxidation states. Examples

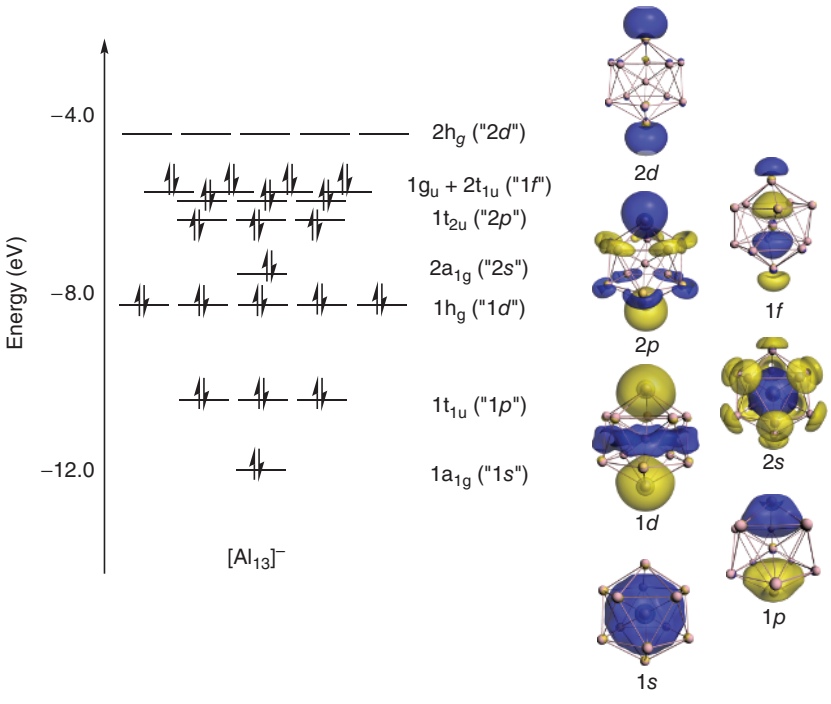

Figure 1.4 The icosahedral $[Al_{13}]^-$ cluster: a "superhalide."

of metal–metal bonds are limited to heterobimetallic cases where the lanthanide acts as a Lewis acid in combination with strongly Lewis basic transition metal fragments such as $[Fe(CO)_4]^{2-}$ or $[Ru(Cp)(CO)_2]^-$. In $(Cp)_2Lu(thf)$-$Ru(Cp)(CO)_2$, for example, the interaction between the metals is primarily electrostatic (Lu–Ru 2.995(2) Å) [37], the HOMO having <10% Lu character. A similar electrostatic picture emerges even in adducts of the earlier lanthanide ions such as Nd^{III}, where the f shell is higher in energy and only partly filled [38]. The more diffuse 5f orbitals of the actinides allow higher oxidation states to be accessed and, in principle, also allow the f orbitals to participate directly in the bonding. Substantial charge transfer from an $Al(\eta^5\text{-}C_5Me_5)$ unit to U^{III} has been reported in $(\eta^5\text{-}C_5H_4\text{–}SiMe_3)_3U\text{–}Al(\eta^5\text{-}C_5Me_5)$ [39], and there is even some evidence for weak π overlap involving the 5f orbitals in the U–Re bond in $[\{N(CH_2CH_2NSiMe_3)_3\}URe(\eta^5\text{-}C_5H_5)_2]$ and the U–Ga bond in $[(Tren^{TMS})U\{Ga(NArCH_2)_2\}(THF)]$ [40]. The role of the 5f orbitals is, however, a relatively minor component of the bonding in all cases.

1.3 Metal–Metal Bonds Involving d Orbitals

Over the past 50 years, the three transition series have been responsible for the vast majority of metal–metal bonded species, and an enormous number of dimers and larger clusters are now known. In addition to providing a unique insight into the nature of the chemical bond, these clusters have been exploited for their catalytic potential [7], and a biological role for a Ni–Fe bond in Ni–Fe hydrogenases has even been proposed [8]. Transition metal–metal bonds may be broadly classified into two types: "supported" bonds that have ligands that bridge the two centers and "unsupported" bonds that do not. In the supported class, the relative importance of metal–metal and metal–ligand interactions is often difficult to delineate because any single molecular orbital may feature contributions from both. On the other hand, the presence of bridging ligands confers great flexibility, simply because the

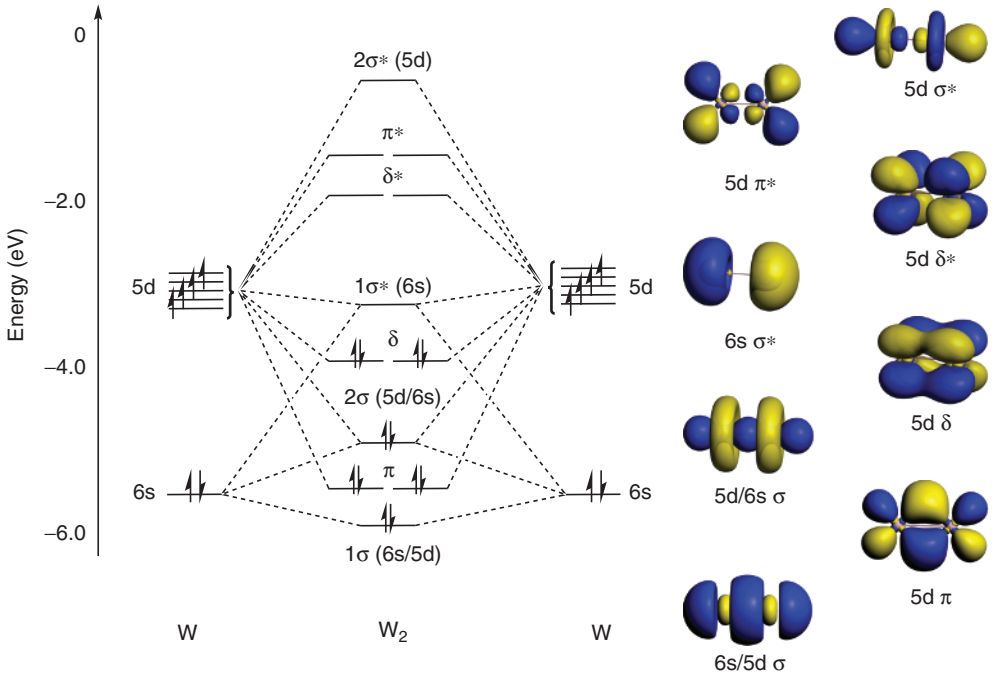

Figure 1.5 The singlet ground state of sextuply bonded W_2.

cluster does not rely solely on the metal–metal bond for its integrity. The limit of negligible direct overlap of the metal orbitals corresponds to the extensive class of exchange-coupled clusters, which lie outside the remit of this book. There are, however, a few intermediate cases where the metal–metal bond is partially formed, and even cases where distinct bonded and nonbonded isomers can be isolated [41, 42].

A survey of the electronic structure of the naked transition metal diatomics, M_2, serves to highlight many of the key periodic trends that emerge in their more chemically relevant ligated analogs. The diatomics encompass a wide range of metal–metal bond types, from strong multiple bonding to weak magnetic coupling, and they have been used as a testing ground for successive generations of theoretical methods. The elements near the center of the transition series are the most interesting from a bonding perspective as they offer the potential for extreme high bond orders, up to six in the dimers of the group VI metals Cr_2, Mo_2, and W_2. The molecular orbital array for W_2, the heaviest member of the series, illustrated in Figure 1.5 illustrates the basic features of the sextuple bond: the doubly degenerate π and δ components are supplemented by *two* distinct orbitals with σ symmetry, 1σ and 2σ, each with mixed $5d_{z^2}$/6s character. 2σ represents a conventional σ bonding orbital, in so much as the dominant $5d_{z^2}$ character is concentrated along the internuclear axis. In 1σ, in contrast, the dominant 6s character concentrates the overlap in a cylindrical region around the axis, reducing electron–electron repulsions with the 2σ component. The $5d_{z^2}$/6s hybridization is closely related to the Orgel/Dunitz mechanism used to account for the preference for linear coordination in complexes of the coinage metals [43].

The formal bond order of 6 in W_2 reflects the structure of the molecular orbital diagram but is clearly simplistic in that it fails to take into account the very different contributions of the σ, π, and δ components to the overall bond strength. In the case of the δ bonds in particular, the weak overlap leads to a small HOMO–LUMO gap, and the single determinant description of the electronic structure that is implicit in the molecular orbital diagram can be inadequate. Within the constraints of single determinant methods such as DFT, the weakness of the δ bond (and, to a lesser extent, the π

component) manifests itself in a tendency toward symmetry breaking, wherein electrons of opposite spin localize on different centers. For example, Bauschlicher's study of Cr_2 revealed net spin densities of ±2.7 at opposite centers, reflecting the strong tendency of the electrons in both the δ and π bonds to localize [44]. The potential energy surface for Cr_2 also highlights a link to the main group species discussed previously. A minimum at the equilibrium separation of 1.67 Å allows for substantial 3d–3d overlap, but a plateau is also present in the region of 2.5 Å, a result of residual overlap between the more diffuse 4s orbitals. The bonding in this region is in fact very reminiscent of that in the Mg_2^I and Zn_2^I dimers, in so much as 4s–4s overlap is the dominant feature: the three systems differ only in the size of the spherically symmetric 3d cores: d^0, d^5, and d^{10} for $Mg^I{}_2$, $Cr^0{}_2$, and $Zn^I{}_2$, respectively. Multiconfigurational character also becomes apparent in CASSCF calculations, where the effective bond orders of 5.2, 5.2, and 4.52 for W_2, Mo_2, and Cr_2, respectively, highlight the weakness of the δ component, particularly in the lightest member of group 6 [45]. In Mn_2, the five 3d electrons on each center are again weakly antiferromagnetically coupled, but both in- and out-of-phase combinations of the 4s orbital are now doubly occupied. Mn_2 can therefore be viewed as an analog of an inert gas dimer, where the bonding is dominated by van der Waals' forces, and the Mn–Mn separation in the $^1\Sigma_g^+$ ground state has been estimated at 3.64 Å [46]. Perhaps unsurprisingly this situation presents a substantial challenge to DFT, and computed Mn–Mn separations ranging from 1.6 to 3.5 Å have been reported [47].

The increasing strength of bonds involving nd orbitals down a group is a general feature of transition metal chemistry, the origins of which lie in the more diffuse nature of the 4d and 5d orbitals relative to s and p orbitals with the same principal quantum number: the greater exposure of the nd orbital *increases* diatomic d–d overlap from its very low value in the first transition series. A quantitative understanding of periodic trends, however, also requires an appreciation of the changes in electron–electron repulsion as the bond is formed. In the limit of very weak bonding (for example, as in the Mn_2 case), the individual atoms adopt local high-spin configurations, thereby minimizing electron–electron repulsions. The sharing of electron density in covalent bonds necessarily equalizes the spin densities at the two atoms, causing an increase in electron–electron repulsion. Thus, covalent bonding represents a compromise between overlap, which lowers the kinetic energy and so favors bond formation and the competing increase in electron–electron repulsions. The latter are largest in the compact 3d orbitals, and so in addition to the weak overlap, the lighter elements experience a greater increase in electron–electron repulsion upon formation of a covalent bond. A detailed analysis suggests that the two factors contribute approximately equally to the overall trend to stronger metal–metal bonds in the heavier transition elements [48, 49].

An introduction to metal–metal bonding in the transition metals would be incomplete without a discussion of the iconic quadruple bond in $[Re_2Cl_8]^{2-}$. This molecule represents a major landmark in inorganic chemistry, simply because the δ component of the bond was entirely without precedent in the main group. The quadruple bond has subsequently become synonymous with the field of metal–metal bonding, and its structure and properties have been extensively reviewed, most prominently in the seminal textbook "*Multiple Bonds Between Metal Atoms*." [50] The short Re–Re separation and eclipsed nature of the $ReCl_4$ units in an anion formulated as $[Re_2Cl_8]^{4-}$ (in "(pyH)(H)$ReCl_4$") were in fact first noted by Kuznetsov and Koz'min in 1963 [10], but a subsequent study of the potassium compound $KReCl_4.H_2O$ by Cotton and Harris revealed a dianion with an Re–Re distance of 2.241(7) Å, now correctly formulated as $[Re_2Cl_8]^{2-}$ [9]. Very soon afterward, Cotton presented the first electronic rationale for the structure [11], and the essential features of this model underpin all the more sophisticated treatments that have been reported in the subsequent half century. Cotton's model, summarized in Figure 1.6, shows how the electronic structure emerges naturally from perturbations to the diatomic developed in Figure 1.5. The combination of the high oxidation state (Re^{III}) and the square-planar ligand field removes the 6s and $5d_{x^2-y^2}$ orbitals from the valence manifold, leaving only $5d_{z^2}$, $5d_{xz}$, $5d_{yz}$, and $5d_{xy}$ available to form the Re–Re bond. The σ, π, and δ linear combinations that result from diatomic overlap give rise to a $\sigma^2\pi^4\delta^2$ ground-state configuration with a

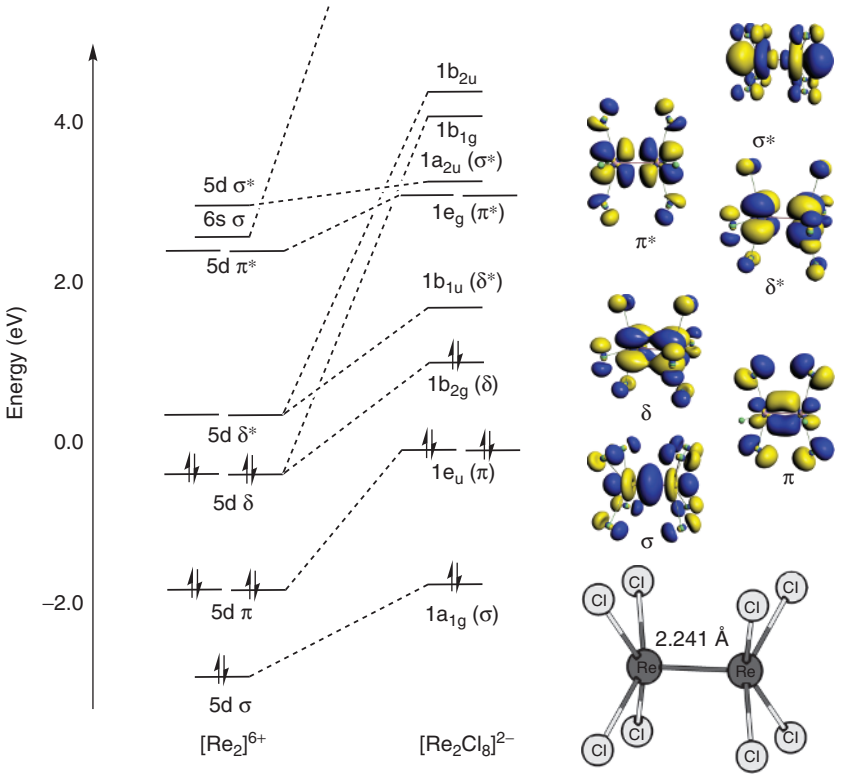

Figure 1.6 The quadruple bond in $[Re_2Cl_8]^{2-}$ (the midpoint of the δ/δ* pair is taken as an arbitrary zero of energy).

formal bond order of 4.0. The δ overlap between the d_{xy} orbitals can account for the adoption of the fully eclipsed conformation, although it has also been argued that hyperconjugation between Re–Cl σ and Re–Cl σ* orbitals contributes to the conformational preference [51].

While the basic features of Figure 1.6 were established by Cotton's 1965 paper, attempts to quantify the strength of the δ bond had to await the emergence of more sophisticated theoretical models [52]. A 1994 CASSCF calculation on $[Re_2Cl_8]^{2-}$ using an (8,8) active space including the Re–Re σ, π, and δ orbitals along with their antibonding counterparts [53] indicated that the lead $\sigma^2\pi^4\delta^2\delta^{*0}\pi^{*0}\sigma^{*0}$ configuration makes up only ~63% of the total wavefunction. This conclusion is consistent with the symmetry breaking apparent in DFT-based studies of the same system [54, 55]. More recently, (8,8) and (12,12) active spaces (the latter including the Re–Cl σ and σ* orbitals) have been used to optimize the geometry of $[Re_2Cl_8]^{2-}$, the resulting Re–Re bond length being in good agreement with X-ray data [56, 57]. The occupations of the δ and δ* orbitals in the CASSCF wavefunction (~1.5 and ~0.5, respectively) confirm the weakness of the δ bond.

While $[Re_2Cl_8]^{2-}$ is certainly the iconic quadruply bonded molecule, a number of isoelectronic analogs have also been reported including the rhenium bromide [58] and iodide [59], as well as the lighter $[Tc_2X_8]^{2-}$ congeners (X = Cl, Br) [60] and the group VI tetraanions $[Mo_2X_8]^{4-}$ and $[W_2X_8]^{4-}$ [61]. In the osmium analogs, $[Os_2X_8]^{2-}$ (X = Cl, Br), where the presence of two additional electrons in the δ* orbital [62, 63] annihilate the δ bond, the OsX_4 units adopt the more sterically favored staggered conformation. The weakness of the δ component of the metal–metal bond also gives rise to somewhat counterintuitive structural changes upon one-electron reduction of $[Tc_2Cl_8]^{2-}$. Both $[Tc_2Cl_8]^{2-}$ (formal bond order 4.0) and $[Tc_2Cl_8]^{3-}$ (formal bond order 3.5) have been structurally

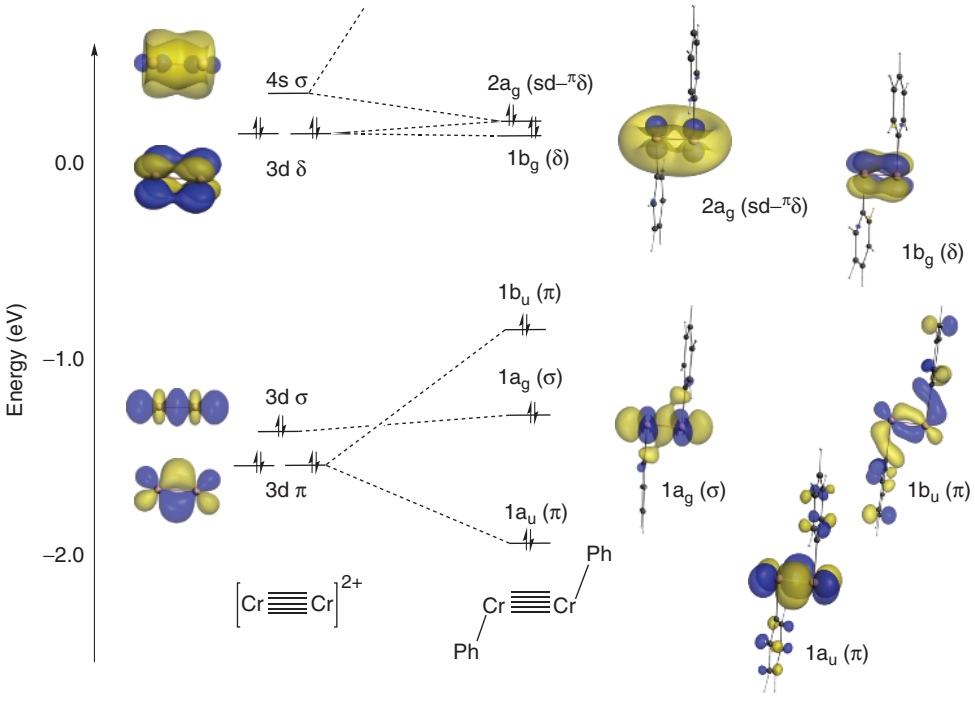

Figure 1.7 Ultrashort Cr–Cr quintuple bonds: correlation of frontier orbitals in $[Cr_2]^{2+}$ and *trans*-bent isomers of Ph–CrCr–Ph (the δ orbital is taken as an arbitrary zero of energy).

characterized, and although bond lengths depend on the identity of the cation, a trend toward shorter Tc–Tc bonds in the trianions can be discerned (2.117(2) vs 2.151(1) Å) [64]. This appears, at first sight, to be surprising as 50% of a δ bond is lost upon reduction. This minor loss of stabilization is, however, more than offset by enhanced overlap in both the σ and π components as a result of the radial expansion of the metal-based 4d orbitals upon reduction. This observation highlights a general theme that will underpin much of the subsequent discussion of bonding in both the transition series and the p-block: σ bonding plays by far the dominant structural role. Indeed, much of the complex structural chemistry to be outlined in the following paragraphs can be understood in terms of optimization of the σ framework, if necessary at the expense of the intrinsically weaker π or δ components of the bond.

Forty years on from the discovery of the quadruple bond in $[Re_2Cl_8]^{2-}$, the range of bond multiplicities in isolable molecules was further extended by Power's synthesis of the landmark compound Ar–CrCr–Ar (Ar = C_6H_3-2,6-(C_6H_3-2,6-^{i}Pr$_2$)$_2$), with a quintuple bond between the metals (Figure 1.7). [1] The Cr–Cr separation of 1.8351(4) Å is extremely short, and the structure is strongly *trans*-bent, with C–Cr–Cr angles approaching 100°. Subsequent work showed that the Cr–Cr distance could be tuned over a narrow range (1.8077(7) – 1.8351(4) Å) by variation in the aromatic substitution pattern [65], the lowest of these values being shorter than the shortest known Cr–Cr quadruple bonds at that time (1.830(4) and 1.828(2) Å) [66]. Soon afterward, a number of closely related "ultrashort" Cr–Cr bonds emerged from the groups of Theopold [67], Kempe [68], and Tsai [69]. The earliest of these reports featured a Cr_2 unit supported by two diazadiene ligands [67], the Cr–Cr separation of 1.8028(9) Å being fractionally shorter than the shortest member of the Ar–CrCr–Ar family. Tsai and Kempe then published almost simultaneous reports of closely related species with even shorter Cr–Cr separations of 1.7397(9) and 1.749(2) Å, respectively, and the current record low of 1.7293(12) Å [70] is held by a complex with a guanidinate ligand architecture. Power's work inspired a number of theoretical studies of the quintuple bond [71 – 76], but its basic features had in fact been

set out some 25 years earlier by Hoffman and coworkers [77], albeit in the context of a perfectly linear L–MM–L, where the distinction between σ-, π-, and δ-symmetric orbitals is rigorous. The analysis of the bonding in Ar–CrCr–Ar is complicated by the *trans* bending, but nevertheless, one σ ($1a_g$ in Figure 1.7) two π ($1a_u$, $1b_u$), and one δ ($1b_g$) component are readily identified in the occupied manifold. The nature of the fifth component of the bond, $2a_g$, is less obvious: like the σ orbital, it is a basis for the totally symmetric representation of the C_{2h} point group, but nevertheless it has been argued that it should be identified loosely as a δ bond. The overlap between the two s/d_{z^2} hybrids is clearly very weak and the $2a_g$ orbital has been labeled as a "side-on δ bond" or "sd-$^{\pi}$δ" to emphasize its qualitative similarity to an orbital of pure δ symmetry [74]. The relationship to the naked $[Cr_2]^{2+}$ dimer shown in Figure 1.7 highlights the reasons why a *trans*-bent structure is energetically favorable. The naked dimer presents two orbitals of σ symmetry, $1\sigma_g$ and $2\sigma_g$, that could, in principle, accommodate the developing Cr–C bond (note that the positive charge stabilizes nd relative to (n + 1)s, so unlike the case for W_2, the (n + 1)s character is more pronounced in the vacant $2\sigma_g$). Approach along the Cr–Cr axis would destabilize the $1\sigma_g$ orbital and, therefore, compromise the strongest component of the Cr–Cr bond. A *trans*-bent approach, in contrast, introduces overlap with the cylindrical $2\sigma_g$ orbital as well as one component of the δ pair, and, therefore, has much less impact on the Cr–Cr interaction. The bending therefore allows the Cr–Ar σ bonds to be established without compromising the energetically most important σ component of the Cr–Cr bond. The driving force for a *trans*-bent structure is therefore the retention of the σ bonding framework: the concomitant destabilization of the π and δ components is of lesser importance. A broader survey of structural possibilities in the model compound HWWH indicates that the quintuple bond is in fact rather resilient, persisting across a wide range of isomers of the M_2L_2 unit, including not just the *trans*-bent structure but also *cis*-bent (C_{2v}), dibridged (D_{2h}), and mono-bridged (C_s) alternatives [76]. The qualitative bonding model that emerges from DFT has been confirmed by a CASPT2 study by Brynda *et al.* [73] where one σ, two π (one in-plane, one out-of-plane), and one conventional δ bond are included in the active space, along with the "sd-δ" side-on δ bond [74]. The antibonding components of both the conventional and side-on δ bonds are substantially populated (0.50 electrons for the former, 0.31 electrons for the latter), leading to an effective bond order of 3.52, well below the idealized limit of 5.0. Nevertheless, the authors conclude that the formation of the Cr–Cr bond does involve five pairs of electrons from each PhCr unit, and, therefore, that the "quintuple" label is justified for bonds of this type. The details of the bonding in the ultrashort Cr_2 species reported by Theopold, Tsai, and Rempe have also been analyzed in some detail [78], and in general rather similar features emerge despite the increase in coordination number at the metal centers. In the dibridged amidinate (Tsai, Kempe), pyridylamide (Kempe), and diazabutadiene (Theopold) analogs and also the lantern $Cr_2(LL)_3$ structure, the metal–ligand interaction is established primarily through the cylindrical s/d_{z^2} hybrid σ orbital of the naked dimer, which has maximum amplitude orthogonal to the Cr–Cr axis, along with one or two components of the δ bond. The Cr–Cr quintuple bond is then formed through one σ, two π, and one δ bond, supplemented either by a second degenerate δ component ($Cr_2(LL)_3$) or a "side-on δ" orbital of the type described above. [78]

Closely related to the M_2X_8 family are the so-called paddlewheel complexes, where the two metal centers are bridged by four chelating ligands. Within this diverse series, the metal–metal interactions fluctuate widely, from the very strong (Mo–Mo = 2.093(1) Å in $Mo_2(O_2CCH_3)_4$) [79] to the very weak (Cu–Cu = 2.6143(17) Å in $Cu_2(O_2CCH_3)_4(H_2O)_2$) [80]. The quadruple bond in $Mo_2(OAc)_4$ is strikingly similar to that in isoelectronic $[Re_2Cl_8]^{2-}$ (Figure 1.6), with the typical $\sigma < \pi < \delta$ ordering of occupied orbitals. Higher valence electron counts demand occupation of the antibonding δ* and π* orbitals, and it is here that the contrasts with the homoleptic M_2X_8 species are most apparent. In the latter, each ligand carries two orthogonal doubly occupied p orbitals (lone pairs), which leads to the destabilization of both the π- and δ-symmetry orbitals on the M_2 unit. In the paddlewheel complexes, in contrast, only the p orbital orthogonal to the M–M axis remains available for π bonding to the metal, the other being involved in σ bonding within the ligand framework. As a result, only the δ-symmetry orbitals of the M_2 unit are destabilized by π-donation from the ligand, reducing and even, in some cases, inverting the δ*–π* separation (Figure 1.8). The near degeneracy of the δ* and π* levels

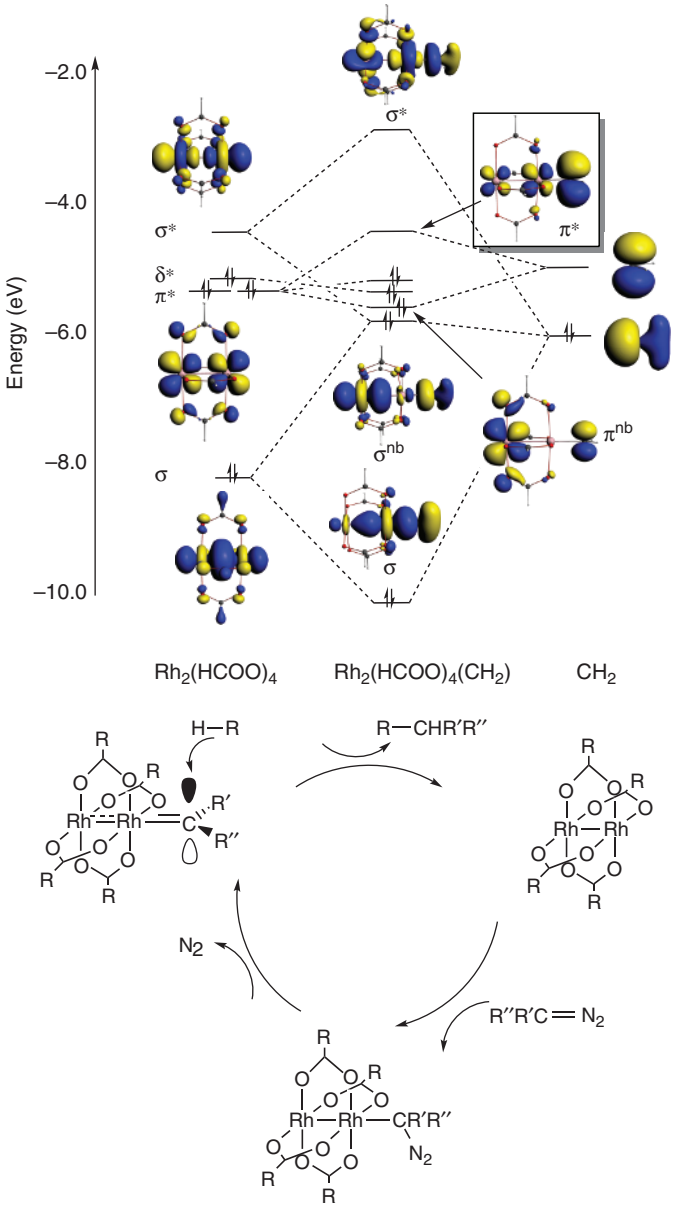

Figure 1.8 Relationship between electronic structure and catalytic activity in the dirhodium carbene complex $Rh_2(HCOO)_4(CH_2)$.

in the paddlewheel complexes has a dramatic impact on their magnetic properties: while $[Os_2Cl_8]^{2-}$ has a $\sigma^2\pi^4\delta^2\delta^{*2}$ singlet ground state, isoelectronic osmium paddlewheel complexes are triplets with either $\sigma^2\pi^4\delta^2\delta^{*1}\pi^{*1}$ or $\sigma^2\pi^4\delta^2\pi^{*2}$ configurations [81].

A further increase in the d-electron count to 14 brings us to the dirhodium paddle wheels ($Rh^{II}{}_2$) that have found extensive use as catalysts for the decomposition of organic diazo compounds and the subsequent insertion of the carbene group into a C–H bond [7]. The complete occupation of the δ/δ*

and π/π* components of the manifold leaves a single Rh–Rh bond ($\sigma^2\pi^4\delta^2\delta^{*2}\pi^{*4}$) with Rh–Rh separations in the region of 2.4 Å. The consensus mechanism for catalysis involves the binding of the carbon of the diazo compound to one Rh center, followed by loss of N_2 to generate the key intermediate, a paddlewheel complex containing a linear Rh–Rh=CR_2 group. Electrophilic attack of the substrate C–H or C=C bond then leads to insertion of the carbene group. The utility of these paddlewheel complexes is related in part to the robust nature of the Rh_2L_4 unit, but also to the subtle interplay between Rh–Rh and Rh–C bonding, which must play a role because insertion into C–H bonds is not a typical reactivity pattern for mononuclear carbenes. By analogy to the Fischer carbenes, the Rh–C bond in the intermediate contains σ- and π-symmetry components generated by the transfer of electron density to and from the bimetallic unit, respectively. The Rh–Rh π* orbital acts as a source of electron density to stabilize the Rh=CR_2 bond, which at the same time allows the Rh–Rh bond to develop some π character. The unique reactivity of the Rh_2 dimers appears to stem primarily from the three-center four-electron nature of the σ bonding in Rh–Rh=CR_2, which weakens the σ component of the Rh=C bond compared to monometallic analogs [82]. Alternatively, this phenomenon can be viewed in terms of the strong *trans* influence of the Rh–Rh bond. The weak, relatively long Rh=C bond in turn localizes the LUMO on the carbene unit (see boxed orbital in Figure 1.8), rendering the latter more susceptible to electrophilic attack. The potential for electron density to flow from the bimetallic core to the bound substrate and back again during the reaction cycle is clearly an important feature of the compound's reactivity.

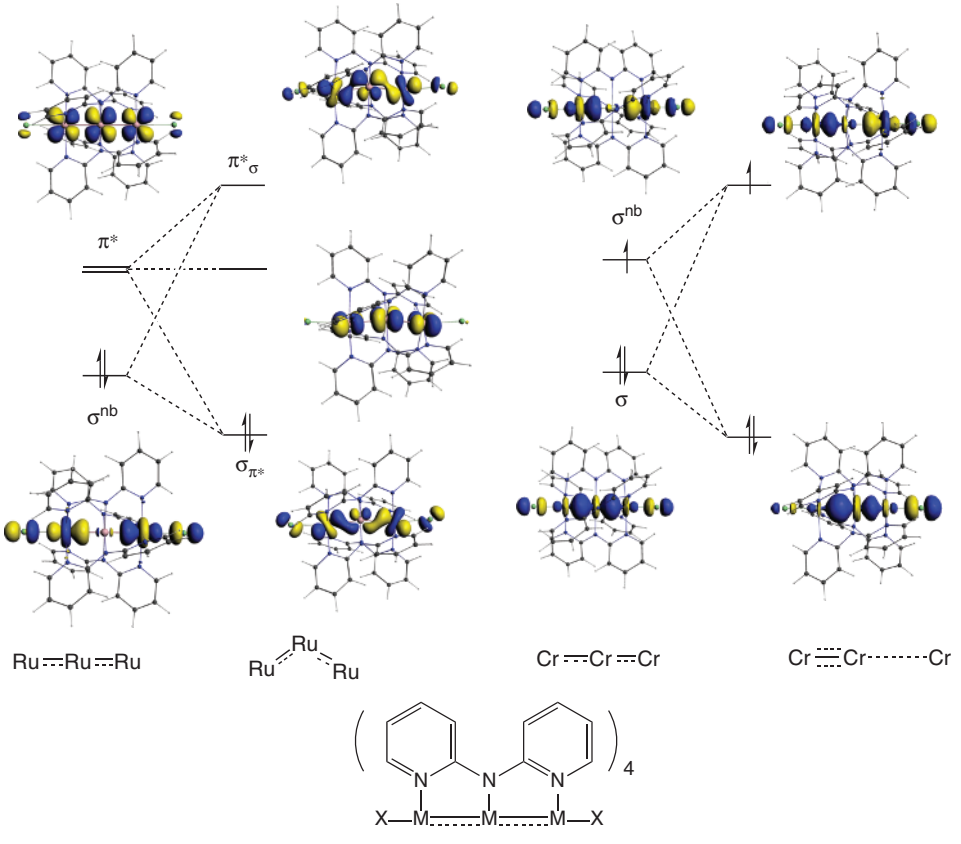

Figure 1.9 Origin of the bends and stretches in $Ru_3(dpa)_4X_2$ and $Cr_3(dpa)_4X_2$.

In recent years, there has been a concerted effort to extend the paddlewheel and related architectures to longer chains. Perhaps the most diverse of these are the so-called extended metal-atom chains (EMACs) developed by Peng, Cotton, and Berry [83, 84]. The archetypes are the trimetallic chains based on a helical array of four dipyridylamide (dpa) ligands, $M_3(dpa)_4X_2$ (Figure 1.9). Complexes of this general formula are now known for much of the first transition series as well as many of the heavier transition elements. The four dipyridylamido ligands provide a scaffold for strong multiple Mo–Mo bonds such as those in $Mo_2M'(dpa)_4X_2$ [85] (M′ = Mn, Fe, Co, Ni, Zn) all the way through to the weak magnetic coupling present in the Ni_3 and Cu_3 analogs [86]. The synthetic strategies used to generate the dipyridylamido ligands are readily extended to analogs with up to 11 nitrogen donor atoms, and metal-atom chains of this length have been reported [87]. The molecular orbital arrays of these chains show the same basic features as the bimetallic paddle wheels, with orbitals of σ, π, and δ symmetry made up of linear combinations of the d_{z^2}, (d_{xz},d_{yz}), and d_{xy} orbitals, respectively. The π and δ components overlap only weakly and form relatively narrow bands, while the σ components show a greater dispersion. This often leads to a densely populated region around the Fermi level, with π* and δ* orbitals lying very close in energy to nonbonding orbitals of σ symmetry. In such circumstances, second-order effects can lead to distinct low-symmetry distortions, which, in turn, have significant impact on the magnetic and electron transport properties [6]. In the triruthenium EMACs $Ru_3(dpa)_4X_2$, for example, a truly linear Ru_3 unit is found only when X is a strong σ donor ligand (CN^- or RCC^-): otherwise, a distinct bending at the central Ru atom occurs (Ru–Ru–Ru ~ 170°) [85]. A closely related phenomenon occurs in the trichromium analogs, $Cr_3(dpa)_4X_2$, where again only strong σ donors such as CN^- and RCC^- yield truly symmetric structures. At the opposite extreme, $Cr_3(dpa)_4(NO_3)_2$ retains a linear Cr_3 unit (Cr–Cr–Cr = 180°), but the Cr–Cr separations themselves are now grossly asymmetric (ΔCr–Cr = 0.71 Å). Intermediate cases such as $Cr_3(dpa)_4Cl_2$ (ΔCr–Cr = 0.22 Å) [88, 89], and $Cr_3(dpa)_4(NCS)_2$ (ΔCr–Cr = 0.25 Å) are also known [90]. Both types of distortion can be understood in terms of the primacy of the σ bonding framework over the weaker π or δ components. In the Ru_3 case, the linear structure has a formal bond order of 3.0 (1.5 *per* Ru–Ru bond), made up of $1\sigma + 2\pi$ components. Bending introduces mixing between the near degenerate σ^{nb} and π* orbitals, increasing the σ character in the Ru–Ru bonds at the expense of π [91]. In the Cr_3 case, second-order effects mix σ and σ^{nb} orbitals, driving an asymmetric stretch rather than a bend. The distortion generates one very strong Cr–Cr bond along with an isolated Cr^{II} center ($S = 2$) [92]. Stronger σ donor ligands such as CN^- again dampen the second-order effects by destabilizing the σ^{nb} orbital: in effect, the formation of a short, strong Cr–Cr σ bond becomes unfavorable because it compromises the strong *trans* Cr–L bond.

One of the main motivations for the synthetic effort invested in these extended metal-atom chains is the search for molecular analogs of the semiconductor-based wires, diodes, and transistors that are the building blocks of present day computers. Peng, Chen, and coworkers have made extensive use of conductive atomic force microscopy (CAFM) and scanning tunneling microscopy (STM) techniques to establish important periodic trends in the conductance (G) across a range of EMACs [90, 93]. For example, conductivity increases in the order Ni < Co < Cr, irrespective of the chain length, suggesting a direct link between electronic configuration and current. By analogy with organic conductors, it is tempting to ascribe the higher conductance of the Cr chains to the presence of π interactions, but a detailed analysis of $Cr_3(dpa)_4(NCS)_2$ indicates that it is dominated by a channel of σ symmetry [94], which lies close the Fermi level of the electrode. The complex nature of the metal–metal bond clearly makes it difficult to extrapolate structure–property relationships from organic materials, but future progress will rely heavily on models that link transport properties to the underlying electronic structure.

Much like the paddlewheel structures, face- and edge-shared bioctahedral complexes (M_2X_9) are also found across much of the transition block, and they illustrate very elegantly many of the important periodic trends. Metal–metal separations span almost 1 Å in the nonachloride series alone, mapping out a continuum linking entirely nonbonded situations (as in $[Rh_2Cl_9]^{3-}$ and $[Ir_2Cl_9]^{3-}$, M–M > 3.0 Å) [95] to strong multiple bonds ($[W_2Cl_9]^{3-}$, W–W = 2.4329(6) Å) [96]. The qualitative features of the molecular orbital array for this class, established using extended Hückel theory and

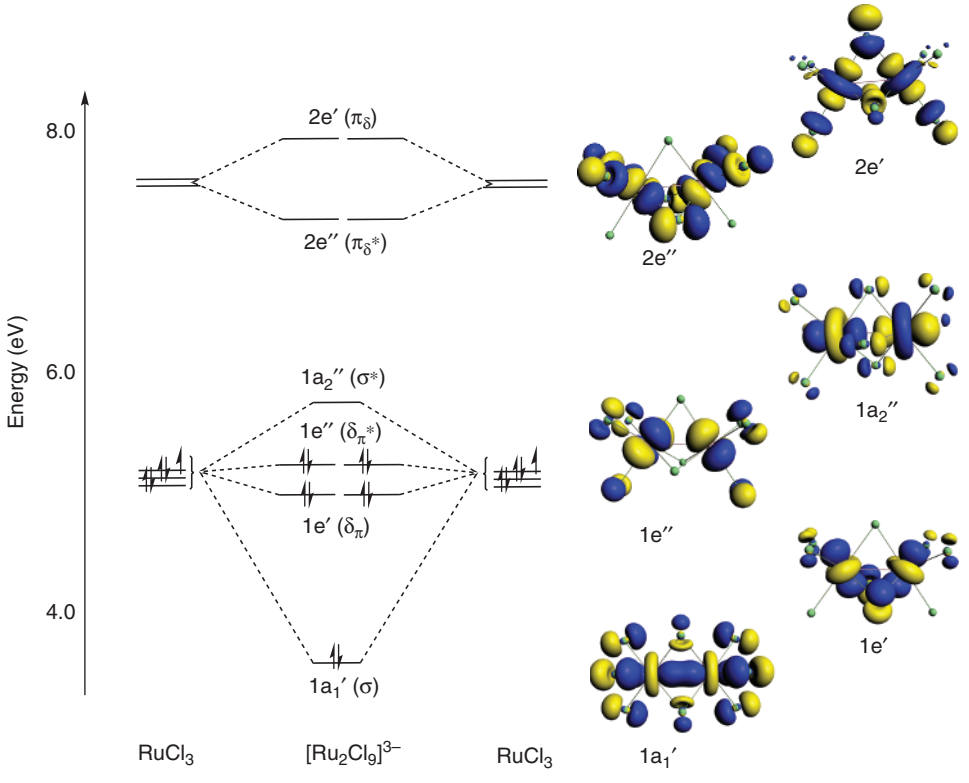

Figure 1.10 $[Ru_2Cl_9]^{3-}$, the archetype of the M_2X_9 family.

DFT methods [97–99], are summarized for the archetype $[Ru_2Cl_9]^{3-}$ (Ru–Ru = 2.725 Å) [100] in Figure 1.10. The threefold degenerate orbitals of a $RuCl_3$ fragment are conveniently quantized along the trigonal axis, leading to one level with σ symmetry (made up of d_{z^2}) and a degenerate pair with mixed π/δ symmetry ($2/3\pi + 1/3\delta$ in a perfect bioctahedron). Combination of the two fragments then leads to σ, σ*, δ_π, and δ_π* levels, which can strongly mixed with p orbitals of the three bridging halides. The isosurfaces shown in Figure 1.10 emphasize the important point that metal–metal and metal–ligand π bonding are antagonistic: the σ and δ_π orbitals are simultaneously Ru–Ru bonding and Ru–Cl antibonding. In cases where the Ru–Ru overlap is inherently weak, as for example in the upper π_δ set, the Ru–Cl antibonding character can invert the expected order, with the out-of-phase combination (2e″) lying lowest. In the closely related di-chloro bridged ruthenium dimer $(CpClRu)_2(\mu\text{-}Cl)_2$, the metal–metal and metal–ligand bonding is in fact so finely balanced that two distinct isomers with Ru–Ru distances that differ by 0.8 Å are found in the same crystal [41, 42]. In one, the Ru–Ru σ bond is optimized at the expense of a relatively weak terminal Ru–Cl interaction (Ru–Ru = 2.930(1) Å, $Ru–Cl_t$ = 2.418(2) Å), while in the other the Ru–Cl bonding is optimized at the expense of the Ru–Ru interaction (Ru–Ru = 3.752(1) Å, $Ru–Cl_t$ = 2.365(2) Å).

The effect of changing the electronic configuration can be extrapolated using the framework set out in Figure 1.10. Thus, a d^6d^6 configuration found, for example, in $[Rh_2Cl_9]^{3-}$, populates the σ* orbital and eliminates the direct Rh–Rh bond. The equilibrium Rh–Rh separation of 3.121(5) Å then represents a balance between the confining influence of the three bridging ligands and the coulomb repulsion between the Rh^{3+} ions. At the opposite extreme, the d^3d^3 configuration in the $[W_2Cl_9]^{3-}$ anion depopulates the δ_π* orbital, giving a formal bond order of 3. This anion was in fact one of the very earliest bimetallic complexes to be subjected to X-ray structural analysis, as far back as 1935: [97]

the structure clearly revealed the strong bonding between the metal atoms (W–W = 2.4329(6) Å), although its precise origins remained unclear for several decades. The very different contributions of σ, π, and δ components to metal–metal bond strength have been emphasized throughout this chapter, and the complexes of group VI provide a vivid illustration of this point. The very short W–W bond in $[W_2Cl_9]^{3-}$ contrasts with the much larger separation of 3.12 Å in isoelectronic $[Cr_2Cl_9]^{3-}$ [101]. In the latter, the radially contracted 3d orbitals allow minimal diatomic overlap, irrespective of the symmetry of the interaction (σ or δ_π), and the result is almost complete localization of all the valence orbitals. The $[Mo_2Cl_9]^{3-}$ system is an intriguing intermediate case: the metal–metal bond length is highly dependent on the identity of the cation in the $A_3Mo_2Cl_9$ lattice, varying from 2.524 Å (A = K^+) to 2.734 Å (A = pipeH^+) [102]. The potential energy surface in this region is very flat and maps out a transition from a triply bonded situation typified by $[W_2Cl_9]^{3-}$ to one where the σ bond remains intact but the two δ_π components are lost. The triad of $[Cr_2Cl_9]^{3-}$, $[Mo_2Cl_9]^{3-}$, and $[W_2Cl_9]^{3-}$ therefore shows a progressive increase in the effective bond order from 0 through ~1 to ~3. The isoelectronic $[Mo_2Cl_9]^{3-}$ and $[Re_2Cl_9]^{-}$ anions also provide an unusual example of a diagonal relationship in the transition metal block because the Re–Re bond length of 2.704(1) Å [103] in the latter is also indicative of the presence of a single Re–Re σ bond. The greater radial expansion of the 5d orbitals of Re relative to the 4d orbitals of Mo is clearly offset by the increased charge on the Re^{4+} cation, leading to a very similar balance between overlap and exchange energies. The one-electron reduction of $[Re_2Cl_9]^{1-}$ offers a further striking illustration of the points introduced earlier in the context of the $[Tc_2Cl_8]^{2-/3-}$ couple, where one-electron reduction caused a contraction in the bond (albeit a marginal one) despite a reduction in the formal bond order [64]. The Re–Re bond length in $[Re_2Cl_9]^{2-}$ is 2.473(4), 0.23 Å *shorter* than in the monoanion, despite a reduction in the formal bond order from 3.0 to 2.5. The loss of half of a δ_π bond is structurally inconsequential, and the dominant factor is again the increase in σ bond strength associated with the expansion of the 5d orbitals on Re.

The difficulties in identifying an unambiguous metal–metal bond order when bridging ligands are present are further illustrated by a debate in the recent literature concerning the bonding in $Fe_2(CO)_9$ (Figure 1.11) [104, 105]. The 18-electron rule demands that such a bond is present, and, indeed, the Fe–Fe separation of 2.523(1) Å appears consistent with this proposal. It is not clear, however, whether this short separation genuinely reflects a bonding situation, or simply the very small size of the bridging ligands. The local d^8 configuration fills the bonding (σ and δ_π) and antibonding (σ* and δ_π*) combinations as well as the 2e″ (π_δ*) orbital (Figure 1.11), giving a formal bond order of −2 – that is, a net antibond. Hartree–Fock calculations by Bauschlicher [106] and an analysis of the Laplacian of the charge density in $Fe_2(CO)_9$ by Poblet and coworkers [107] appear to corroborate the view that there is no direct Fe–Fe bond present. Mealli and Proserpio argued, also on the basis of the extended Hückel theory and charge density analysis, that interaction of the Fe–Fe σ* orbital with a linear combination of CO π* orbitals with a_2'' symmetry transferred some antibonding character from the $1a_2''$ orbital into the vacant manifold ($2a_2''$ in Figure 1.11), meaning that the Fe–Fe bonding character in $1a_1'$ is in fact not completely offset by the antibonding character in $1a_2''$ [108, 109]. Despite these subtle differences, it seems clear that whatever interaction is present between the Fe centers, it is most certainly *not* a simple covalent sharing of two unpaired electrons on the metals as implied by the 18-electron rule. There are, in fact, many parallels between 34-electron $Fe_2(CO)_9$ and square-planar 16-electron species, not least the tendency of both to react with nucleophiles. The breakdown of the 18-electron rule in square-planar complexes occurs because the vacant p_z orbital fails to find an appropriate symmetry match among the linear combinations of ligand-based orbitals, and so is not used, either to form a bond or to accommodate metal-based lone pairs of electrons. The position of the equilibrium between 16-electron ML_4 and 18-electron ML_5 is then determined by the balance between electron transfer from a fifth ligand into the p_z orbital and repulsion with the filled d_{z^2}, which occupies the same region of space. In $Fe_2(CO)_9$, there are two vacant a_2''-symmetric metal-based combinations (primarily linear combinations of 4s and $4p_z$) but only one occupied ligand-based combination of the same symmetry. Thus, one of the two metal-based orbitals remains "unused" in

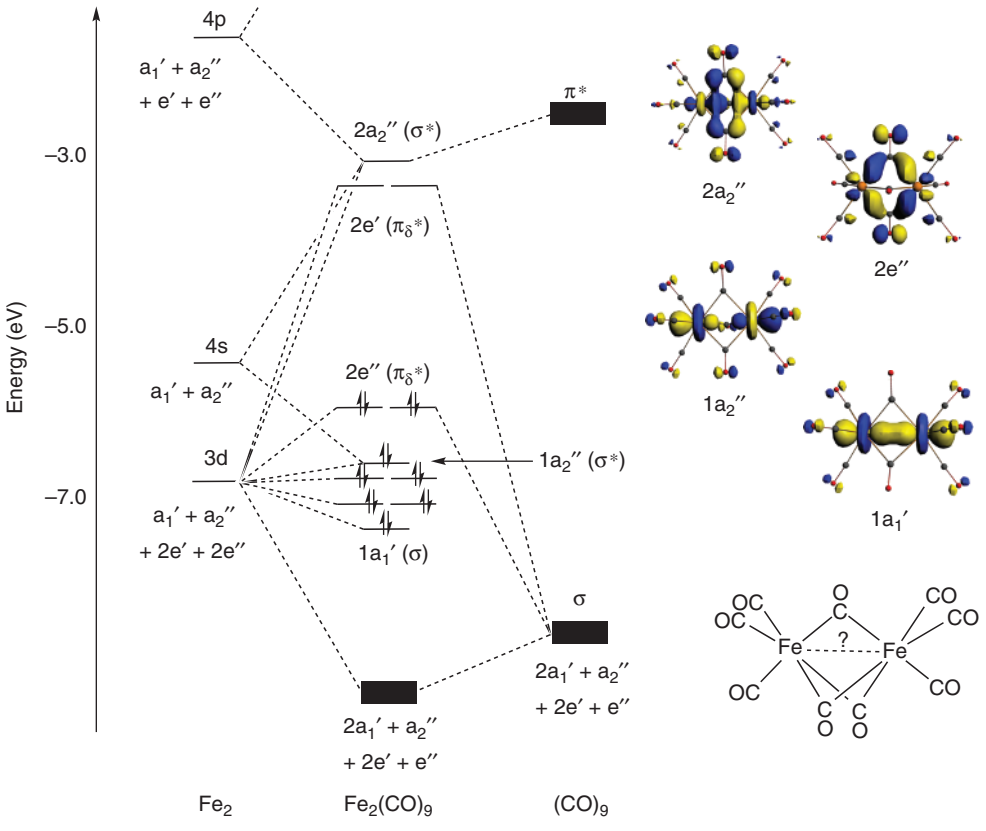

Figure 1.11 $Fe_2(CO)_9$: bond or no bond?

the same sense that the p_z orbital remains unused in square-planar species. This simple symmetry-based analysis suggests that there is no need to invoke an Fe–Fe bond in $Fe_2(CO)_9$ simply because the metal centers do not conform to the 18-electron rule.

1.4 Metal–Metal Bonds Between *f* Orbitals

The relatively weak d–d overlap in the transition series arises because the nd valence orbitals have radial maxima in the same region as their fully occupied ns and np counterparts. The situation is even more exaggerated in the lanthanide and actinide series where the nf valence orbitals are famously "core-like," with radial maxima actually inside the fully occupied {(n + 1)s, (n + 1)p} shells (see Eu in Figure 1.2). The result is that overlap between nf orbitals is negligible and instead strong interactions between ligands and the vacant (n + 2)s orbitals tend to favor highly coordinated monometallic complexes over metal–metal bonded dimers. Indeed, only the actinide series shows any significant homobimetallic chemistry and then only in inert matrices. The naked diatomic U_2 [110] has been characterized by vibrational spectroscopy, as have the hydrides U_2H_2 and U_2H_4 [111]. The electronic structure of the gas-phase diatomic U_2 highlights the complexity of the bonding in this region of the periodic table. A CASSCF study suggests that the ground state is a septet with a dominant configuration $(7s,6d\sigma_g)^2(6d\pi_u)^4(6d\sigma_g)^1(6d\delta_g)^1(5f\delta_g)^1(5f\pi_u)^1(5f\phi_u)^1(5f\phi_g)^1$ and a total orbital angular

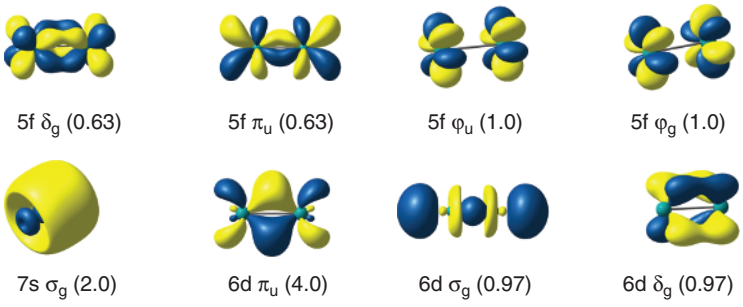

Figure 1.12 Occupations of orbitals in the septet ground state of U_2 (CASSCF).

momentum, Λ, of 11 (the $m_l = +1$, +2, and +3 components of π_u, δ_g, and ϕ_u, respectively, are occupied) (Figure 1.12) [112]. The formal bond order is therefore 5.0, just as in ArCrCrAr, but the nature of the quintuple bond is very different, being composed of three 2-center 2-electron bonds (7s,6dσ_g and doubly degenerate 6dπ_u) and four 2-center 1-electron bonds (6dσ_g, 6dδ_g, 5fδ_g, and 5fπ_u). The remaining two electrons in 5fϕ_u and 5fϕ_g make no net contribution to the bonding.

A very different type of quintuple bond is present in the putative plutonium compound $[Pu_2Cl_8]^{2-}$ (Pu(III), f^5), where the high oxidation state and the presence of a ligand field stabilizes the 5f shell relative to 6d and 7s [113]. The resulting ($\sigma + 2\pi + 2\delta$) quintuple Pu–Pu bond is created primarily through 5f–5f overlap (Figure 1.13). This pair of quintuply bonded species U_2 and $[Pu_2Cl_8]^{2-}$ elegantly highlights the plethora of bonding possibilities when 7s, 6d, and 5f orbitals are near degenerate. A feature of Figures 1.12 and 1.13 is the presence of orbitals with ϕ symmetry (i.e., with *three* angular nodes that contain the internuclear axis), which are unique to atomic orbitals with $l > 2$. There is no net ϕ component to the bonds in either U_2 or $[Pu_2Cl_8]^{2-}$ because the bonding and antibonding combinations are equally occupied in both cases, but a ϕ component has been proposed in the U–U bond in the $^7A_{2u}$ ground state of the encapsulated species $U_2@C_{60}$ (Figure 1.14) [114].

1.5
Metal–Metal Bonds Between p Orbitals

Moving from the transition series to the p-block, we return to the typical main group situation where the valence orbitals (in this case ns and np) are radially diffuse relative to other occupied orbitals (Sn, Figure 1.2). The diatomic overlap in the lighter elements is therefore close to optimal and decreases as the principal quantum number increases. The result is a general reduction in bond strength in the heavier elements, precisely the opposite trend to that observed in the transition series. A second significant consideration in this region of the periodic table is the increase in the separation of the ns and np orbitals with atomic number, causing the ns orbital to become core-like (the inert-pair effect). The bonding interactions, conversely, are increasingly dominated by the p orbitals, driving a preference for bond angles approaching 90° rather than the larger values of 109.5°, 120°, or 180° favored when s and p contribute more equally. The impact of these periodic trends in the context of metal–metal bonds is exemplified by the heavier analogs of alkenes and alkynes, the first of which was Lappert's distannene $Sn(CH(SiMe_3)_2)_2$, with a Sn=Sn bond length of 2.768(1) Å. [115] Prior to this, the so-called double-bond rule, the observation that multiple bonds were stable only between elements of the first long period [116], appeared to be universally valid. Other doubly (Si=Si [117], Ge=Ge [118], and Pb=Pb [119]) and triply (Sn≡Sn [4] and Pb≡Pb [5]) bonded species have subsequently emerged, the latter only in the last decade. Like the CrCr quintuple bond described previously, their isolation owes much to the creative ligand design, and in particular to the steric bulk of the aryl ligands [120]. The status of the Sn and Pb dimers as doubly or triply bonded analogs of the alkenes or alkynes has been controversial because, much like the quintuply bonded ArCrCrAr,

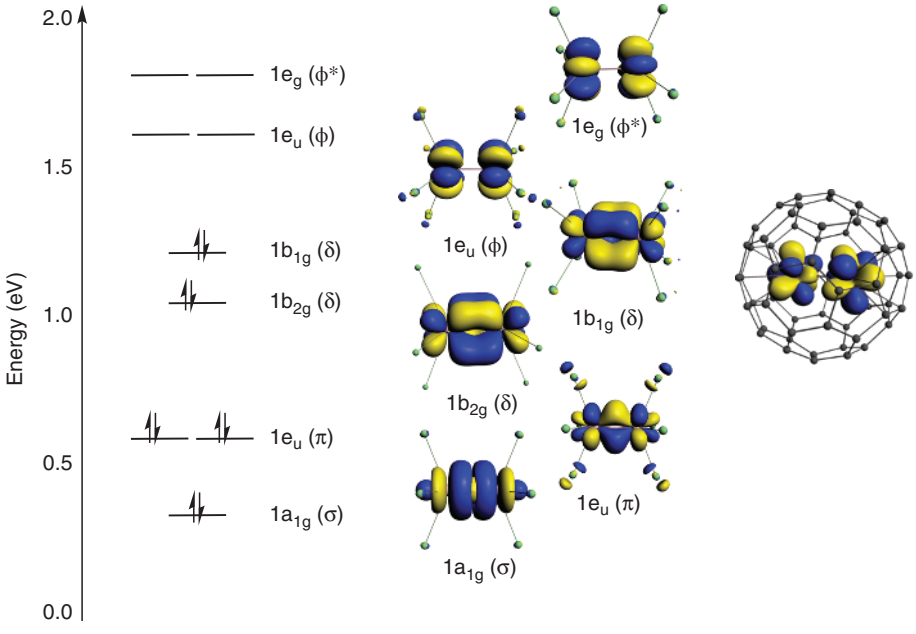

Figure 1.13 The quintuple bond in $[Pu_2Cl_8]^{2-}$ and ϕ overlap in $U_2@C_{60}$.

they are strongly "*trans*-bent." [74] The identification of a formal bond order is therefore complicated by the lack of a rigorous symmetry-based distinction between orbitals of σ and π symmetry. The angle between the R_2M plane and the M–M axis in the alkene analogs is ~40° (compared to a value of 0° for the planar alkene geometry) while the H–M–M angle in the alkyne analogs is ~125° for the Sn systems and ~95° for the heaviest Pb system (Figure 1.14). Similarly, while the Sn=Sn and Sn≡Sn distances are marginally smaller than those in single-bonded analogs, the Pb=Pb and Pb≡Pb bonds are generally considerably longer than typical Pb–Pb single-bonded distances. A number of theoretical models have emerged to explain these periodic trends in M=M and M≡M bonding, all of which have their roots in the increased radial and energetic separation of the ns and np valence orbitals on descending the group. In the planar isomer of the distannene $Me_2Sn{=}SnMe_2$, a conventional σ + π picture of the double bond emerges, albeit with a small HOMO–LUMO gap separating the π and σ* orbitals (Figure 1.14). This planar arrangement means that three σ bonds at each metal center utilize only two of the 5p orbitals, along with some 5s contribution, the third 5p orbital being used exclusively to establish the inherently weak π component of the bond. *Trans* bending allows mixing between the π* and σ* orbitals (a second-order Jahn–Teller distortion) to form a slipped sp- // π bond, which ultimately becomes a nonbonding "resonating lone pair" (resonance structure II in Figure 1.14). The net effect of the *trans* bending is to sacrifice the intrinsically weak π component of the bond in order that the three σ bonds at each center (Sn–Sn + 2 Sn–R) can be formed from three orthogonal p orbitals. In this context, the Sn=Sn bond should be compared to the quintuply bonded ArCrCrAr, where *trans* bending similarly avoids the situation where the two strongest bonds (Cr–Cr σ and Cr–C σ) share the same orbital. Closely related arguments apply to the triply bonded distannynes and diplumbynes, where the *trans* bending affords two orthogonal σ bonds (E–E and E–C) along with a lone pair with dominant ns character. The balance between the various resonance forms in the acetylene analogs is a delicate one, and, at least for the distannynes, a significant contribution from the diradical structure (II in Figure 11.4) has been proposed [121].

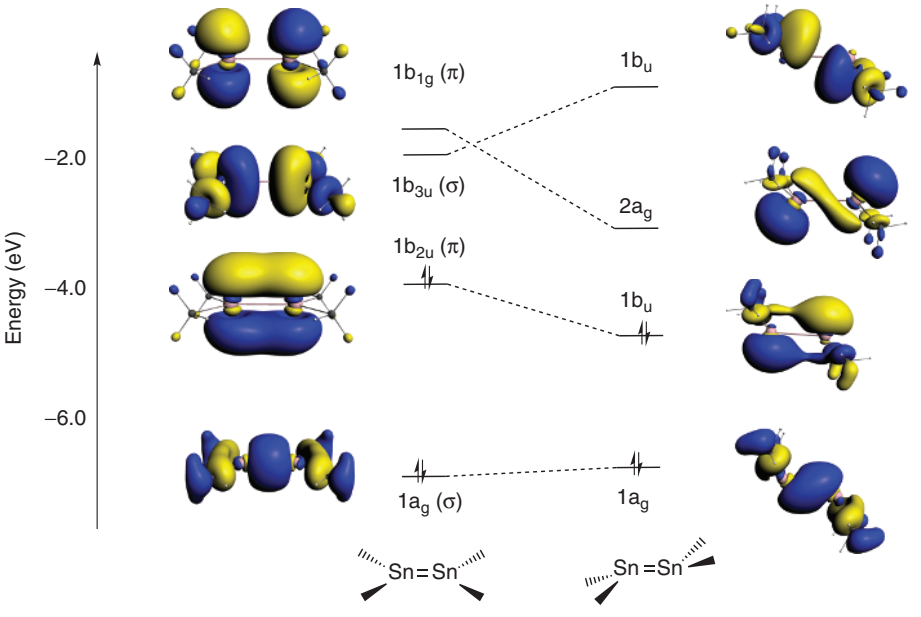

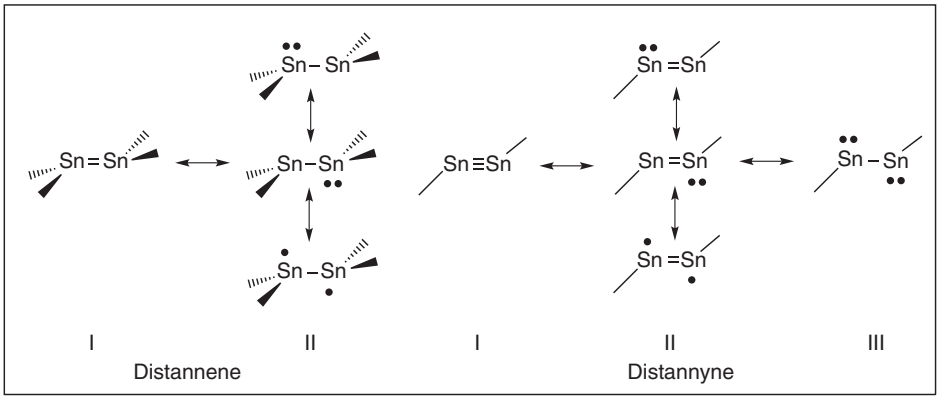

Figure 1.14 *trans* bending in distannenes and distannynes: correlation between planar (D_{2h}) and *trans*-bent (C_{2h}) limits.

1.6 Concluding Remarks

This introductory chapter tries to convey a sense of the diversity of interactions that fall under the broad umbrella of "metal–metal bonds." The quadruple bond with which the subject is most readily associated represents only a small part of an active and expanding field. At one extreme, the last decade has witnessed the race to ever shorter and stronger multiple bonds while at the other, systems with single metal–metal bonds are finding applications in catalysis and even perhaps biology. There seems little doubt that the chemistry of metal clusters will continue to throw up surprises that challenge theory and that will, ultimately, give us a deeper understanding of the nature of the chemical bond.

References

1. Nguyen, T., Sutton, A.D., Brynda, M., Fettinger, J.C., Long, G.J., and Power, P.P. (2005) *Science*, **310**, 844.
2. (a) Green, S.P., Jones, C., and Stasch, A. (2007) *Science*, **318**, 1754; (b) Stasch, A. and Jones, C. (2011) *Dalton Trans.*, 5659.
3. Resa, I., Carmona, E., Gutierrez-Puebla, E., and Monge, A. (2004) *Science*, **305**, 1136.
4. (a) Power, P.P. (2007) *Organometallics*, **26**, 4362; (b) Stender, M., Phillips, A.D., Wright, R.J., and Power, P.P. (2002) *Angew. Chem. Int. Ed.*, **41**, 1785.
5. Pu, L., Twamley, B., and Power, P.P. (2000) *J. Am. Chem. Soc.*, **122**, 3524.
6. Georgiev, V.P., Mohan, P.J., DeBrincat, D., and McGrady, J.E. (2013) *Coord. Chem. Rev.*, **257**, 290.
7. (a) Doyle, M.P., Duffy, R., Ratnikov, M., and Zhou, L. (2010) *Chem. Rev.*, **110**, 704; (b) Davies, H.M.L. and Denton, J.R. (2009) *Chem. Soc. Rev.*, **38**, 3061.
8. Kampa, M., Pandelia, M.E., Lubitz, W., van Gastel, M., and Neese, F. (2013) *J. Am. Chem. Soc.*, **135**, 3915.
9. Cotton, F.A. and Harris, C.B. (1965) *Inorg. Chem.*, **4**, 330.
10. Kuznetsov, V.G. and Koz'min, P.A. (1963) *J. Struct. Chem.*, **4**, 49.
11. Cotton, F.A. (1965) *Inorg. Chem.*, **4**, 334.
12. Liddle, S.T. and Mills, D.P. (2009) *Dalton Trans.*, 5592.
13. Goodgame, M.M. and Goddard, W.A. III, (1985) *Phys. Rev. Lett.*, **54**, 661.
14. Losada, J., Alvarez, S., Novoa, J.J., Mota, F., Hoffmann, R., and Silvestre, J. (1990) *J. Am. Chem. Soc.*, **112**, 8998.
15. Köster, H., Thoennes, D., and Weiss, E. (1978) *J. Organomet. Chem.*, **160**, 1.
16. (a) Wang, X. and Andrews, L. (2004) *J. Phys. Chem. A*, **108**, 11511; (b) Tague, T.J. Jr., and Andrews, L. (1994) *J. Phys. Chem.*, **98**, 8611; (c) Köppe, R., Hence, P., and Schnöckel, H. (2008) *Angew. Chem. Int. Ed.*, **47**, 8740.
17. Overgaard, J., Jones, C., Stasch, A., and Iversen, B.B. (2009) *J. Am. Chem. Soc.*, **131**, 4208.
18. Platts, J.A., Overgaard, J., Jones, C., Iversen, B.B., and Stasch, A. (2011) *J. Phys. Chem. A*, **115**, 194.
19. Glaser, R., Waldron, R.F., and Wiberg, K.B. (1990) *J. Phys. Chem.*, **94**, 7357.
20. Jones, C., McDyre, L., Murphy, D.M., and Stasch, A. (2010) *Chem. Commun.*, **46**, 1511.
21. Kan, Y.H. (2009) *THEOCHEM*, **894**, 88.
22. Kerridge, D.H. and Tariq, S.A. (1967) *J. Chem. Soc. A*, 1122.
23. (a) Greene, T.M., Brown, W., Andrews, L., Downs, A.J., Chertihin, G.V., Runeberg, N., and Pyykko, P. (1995) *J. Phys. Chem.*, **99**, 7925; (b) Wang, X. and Andrews, L. (2004) *J. Phys. Chem. A*, **108**, 11006.
24. (a) Kaupp, M. and von Schnering, H.G. (1994) *Inorg. Chem.*, **33**, 4179; (b) Liao, M.-S., Zhang, Q.-E., and Schwarz, W.H.E. (1995) *Inorg. Chem.*, **34**, 5597.
25. (a) del Rio, D., Galindo, A., Resa, I., and Carmona, E. (2005) *Angew. Chem. Int. Ed.*, **44**, 1244; (b) Xie, Y., Schaeffer, H.F. III, and King, R.B. (2005) *J. Am. Chem. Soc.*, **127**, 2818.
26. Carmona, E. and Galindo, A. (2008) *Angew. Chem. Int. Ed.*, **47**, 6526.
27. (a) Wang, Y., Quillian, B., Wei, P., Wang, H., Yang, X.-J., Xie, Y., King, R.B., von Rague Schleyer, P., Schaeffer, H.F. III, and Robinson, G.H. (2005) *J. Am. Chem. Soc.*, **127**, 11944; (b) Wang, X.-J., Yu, J., Liu, Y., Xie, Y., Schaeffer, H.F. III, Liang, Y., and Wu, B. (2007) *Chem. Commun.*, 2363; (c) Fedushkin, I.L., Skatova, A.A., Ketkov, S.Y., Eremenko, O.V., Piskunov, A.V., and Fukin, G.K. (2007) *Angew. Chem. Int. Ed.*, **46**, 4302; (d) Carrasco, M., Peloso, R., Rodriguez, A., Alvarez, E., Maya, C., and Carmona, E. (2010) *Chem. Eur. J.*, **16**, 9754.
28. Li, T., Schulz, S., and Roesky, P.W. (2012) *Chem. Soc. Rev.*, **41**, 3759.
29. Zhu, Z., Wright, R.J., Olmstead, M.M., Rivard, E., Brynda, M., and Power, P.P. (2006) *Angew. Chem. Int. Ed.*, **45**, 5807.
30. (a) Holloway, C.E. and Melnik, M. (1995) *J. Organomet. Chem.*, **495**, 1; (b) Corbett, J.D., Burkhard, W.J., and Druding, L.F. (1961) *J. Am. Chem. Soc.*, **83**, 76.
31. Bravo-Zhivotovskii, D., Yuzefovich, M., Bendikov, M., Klinkhammer, K., and Apeloig, Y. (1999) *Angew. Chem. Int. Ed.*, **38**, 1100.
32. Zhu, Z., Fischer, R.C., Fettinger, J.C., Rivard, E., Brynda, M., and Power, P.P. (2006) *J. Am. Chem. Soc.*, **128**, 15068.
33. Zhu, Z., Brynda, M., Wright, R.J., Fischer, R.C., Merrill, W.A., Rivard, E., Wolf, R., Fettinger, J.C., Olmstead, M.M., and Power, P.P. (2007) *J. Am. Chem. Soc.*, **129**, 10847.
34. (a) Uhl, W. (1988) *Z. Naturforsch. B*, **43**, 1113; (b) Uhl, W. (1993) *Angew. Chem. Int. Ed.*, **32**, 1386.
35. Dohmeier, C., Robl, C., Tacke, M., and Schnöckel, H. (1991) *Angew. Chem. Int. Ed.*, **30**, 564.
36. (a) Leuchtner, R.E., Harms, A.C., and Castleman, A.W. Jr., (1989) *J. Chem. Phys.*, **91**, 2753; (b) Khanna, S.N. and Jena, P. (1994) *Chem. Phys. Lett.*, **219**, 479.

37. Beletskaya, P., Voskoboynikov, A.Z., Chuklanova, E.B., Kirrilova, N.I., Shestakova, A.K., Parshina, I.N., Gusev, A.I., and Magomedov, G.K.-I. (1993) *J. Am. Chem. Soc.*, **115**, 3156.
38. Arnold, P.L., McMaster, J., and Liddle, S.T. (2009) *Chem. Commun.*, 818.
39. Minasian, S.G., Krinsky, J.L., Williams, V.A., and Arnold, J. (2008) *J. Am. Chem. Soc.*, **130**, 10086.
40. Liddle, S.T., McMaster, J., Mills, D.P., Blake, A.J., Jones, C., and Woodul, W.D. (2009) *Angew. Chem. Int. Ed.*, **48**, 1077.
41. Kölle, U., Kossakowski, J., Klaff, N., Wesemann, L., Englert, U., and Heberich, G.E. (1991) *Angew. Chem. Int. Ed.*, **30**, 690.
42. McGrady, J.E. (2000) *Angew. Chem. Int. Ed.*, **39**, 3077.
43. Dunitz, J. and Orgel, L. (1960) *Adv. Inorg. Chem.*, **2**, 1.
44. Gutsev, G.L. and Bauschlicher, C.W. (2003) *J. Phys. Chem. A*, **107**, 4755.
45. Roos, B.O., Borin, A.C., and Gagliardi, L. (2007) *Angew. Chem. Int. Ed.*, **46**, 1469.
46. Cheeseman, M., VanZee, R.J., Flanagan, H.L., and Weltner, J.W. (1990) *J. Chem. Phys.*, **92**, 1553.
47. (a) Shillady, D.D., Jena, P., Rao, B.K., and Press, M.R. (1988) *Int. J. Quantum Chem. Symp.*, **22**, 231; (b) Nayak, S.K., Rao, B.K., and Jena, P. (1998) *J. Phys. Condens. Matter*, **10**, 10863; (c) Nayak, S.K. and Jena, P. (1998) *Chem. Phys. Lett.*, **289**, 473.
48. Poli, R. and Mui, H.D. (1991) *Inorg. Chem.*, **30**, 65.
49. McGrady, J.E., Stranger, R., and Lovell, T. (1997) *Inorg. Chem.*, **36**, 3242.
50. Cotton, F.A. and Murillo, C.A. (2005) *Multiple Bonds Between Metal Atoms*, Springer, Berlin.
51. Krapp, A., Lein, M., and Frenking, G. (2008) *Theor. Chem. Acc.*, **120**, 313.
52. Hay, P.J. (1978) *J. Am. Chem. Soc.*, **100**, 2897.
53. Blaudeau, J.-P., Ross, R.B., Pitzer, R.M., Mougenot, P., and Bénard, M. (1994) *J. Phys. Chem.*, **98**, 7123.
54. (a) Norman, J.G. Jr., and Kolari, H.J. (1975) *J. Am. Chem. Soc.*, **97**, 33; (b) Mortola, A.P., Moskowitz, J.W., Rosch, N., Cowman, C.D., and Gray, H.B. (1975) *Chem. Phys. Lett.*, **32**, 283.
55. Noodleman, L. and Norman, J.G. Jr., (1979) *J. Chem. Phys.*, **70**, 4903.
56. Saito, K., Nakao, Y., Sato, H., and Sakaki, S. (2006) *J. Phys. Chem. A*, **110**, 9710.
57. Gagliardi, L. and Roos, B.O. (2003) *Inorg. Chem.*, **42**, 1599.
58. Cotton, F.A., DeBoer, B.G., and Jeremic, M. (1970) *Inorg. Chem.*, **9**, 2143.
59. Cotton, F.A., Daniels, L.M., and Vidyasagar, K. (1988) *Polyhedron*, **7**, 1667.
60. Preetz, W. and Peters, G. (1980) *Z. Naturforsch*, **35b**, 797.
61. Brenčič, J.V. and Cotton, F.A. (1969) *Inorg. Chem.*, **8**, 7.
62. Agaskar, P.A., Cotton, F.A., Dunbar, K.R., Falvello, L.R., Tetrick, S.M., and Walton, R.A. (1986) *J. Am. Chem. Soc.*, **108**, 4850.
63. Fanwick, P.E., King, M.K., Tetrick, S.M., and Walton, R.A. (1985) *J. Am. Chem. Soc.*, **107**, 5009.
64. (a) Cotton, F.A., Daniels, L., Davison, A., and Orvig, C. (1981) *Inorg. Chem.*, **20**, 351; (b) Cotton, F.A. and Shive, L. (1975) *Inorg. Chem.*, **14**, 2032.
65. (a) Wolf, R., Ni, C., Nguyen, T., Brynda, M., Long, G.J., Sutton, A.D., Fischer, R.C., Fettinger, J.C., Hellman, M., Pu, L., and Power, P.P. (2007) *Inorg. Chem.*, **46**, 11277; (b) Ni, C. and Power, P.P. (2010) *Struct. Bond.*, **136**, 59.
66. (a) Cotton, F.A. and Koch, S.A. (1978) *Inorg. Chem.*, **17**, 2021; (b) Cotton, F.A., Koch, S.A., and Millar, M. (1978) *Inorg. Chem.*, **17**, 2084.
67. Kreisel, K.A., Yap, G.P.A., Dmitrenko, O., Landis, C.R., and Theopold, K.H. (2007) *J. Am. Chem. Soc.*, **129**, 14162.
68. (a) Noor, A., Wagner, F.R., and Kempe, R. (2008) *Angew. Chem. Int. Ed.*, **47**, 7246; (b) Wagner, F.R., Noor, A., and Kempe, R. (2009) *Nat. Chem.*, **1**, 529.
69. Tsai, Y.-C., Hsu, C.-W., Yu, J.-S.K., Lee, G.-H., Wang, Y., and Kuo, T.-S. (2008) *Angew. Chem. Int. Ed.*, **47**, 7250.
70. (a) Noor, A., Glatz, G., Muller, R., Kaupp, M., Demeshko, S., and Kempe, R. (2009) *Z. Anorg. Allg. Chem.*, **635**, 1149; (b) Noor, A. and Kempe, R. (2010) *Chem. Rec.*, **10**, 413.
71. Frenking, G. (2005) *Science*, **310**, 796.
72. Radius, U. and Breher, F. (2006) *Angew. Chem. Int. Ed.*, **45**, 3006.
73. Brynda, M., Gagliardi, L., Widemark, P.-O., Power, P.P., and Roos, B.O. (2006) *Angew. Chem. Int. Ed.*, **45**, 3804.
74. Landis, C.R. and Weinhold, F. (2006) *J. Am. Chem. Soc.*, **128**, 7335.
75. Weinhold, F. and Landis, C.R. (2007) *Science*, **316**, 61.
76. Merino, G., Donald, K.J., D'Acchioli, J.S., and Hoffmann, R. (2007) *J. Am. Chem. Soc.*, **129**, 15295.
77. Dedieu, A., Albright, T.A., and Hoffmann, R. (1979) *J. Am. Chem. Soc.*, **101**, 3141.
78. La Macchia, G., Manni, G.L., Todorova, T.K., Brynda, M., Aquilante, F., Roos, B.O., and Gagliardi, L. (2010) *Inorg. Chem.*, **49**, 5216.

79. Lawton, D. and Mason, R. (1965) *J. Am. Chem. Soc.*, **87**, 921.
80. Brown, G.M. and Chidambaram, R. (1973) *Acta Crystallogr.*, **B29**, 2393.
81. Miskowski, V.M. and Gray, H.B. (1997) *Top. Curr. Chem.*, **191**, 41.
82. Berry, J.F. (2012) *Dalton Trans.*, **41**, 700.
83. Yeh, C.-Y., Wang, C.-C., Chen, C.-H., and Peng, S.-M. (2006) in *Redox Systems Under Nano-Space Control* (ed T. Hirao), Springer, Berlin, 85–117.
84. (a) Berry, J.F. (2005) in *Multiple Bonds Between Metal Atoms* (eds F.A. Cotton, C.A. Murillo, and R.A. Walton), Springer, New York; (b) Berry, J.F. (2010) *Struct. Bond.*, **136**, 669–706.
85. (a) Sheu, J.-T., Lin, C.-C., Chao, I., Wang, C.-C., and Peng, S.-M. (1996) *Chem. Commun.*, **3**, 315; (b) Kuo, C.-K., Liu, I.P.-C., Yeh, C.-Y., Chou, C.-H., Tsao, T.-B., Lee, G.-H., and Peng, S.-M. (2007) *Chem. Eur. J.*, **13**, 1442.
86. Clérac, R., Cotton, F.A., Dunbar, K.R., Murillo, C.A., Pascual, I., and Wang, X. (1999) *Inorg. Chem.*, **38**, 2655.
87. Ismayilov, R.H., Wang, W.-Z., Lee, G.-H., Yeh, C.-Y., Hua, S.-A., Song, Y., Rohmer, M.-M., Bénard, M., and Peng, S.-M. (2011) *Angew. Chem. Int. Ed.*, **50**, 2045.
88. Clérac, R., Cotton, F.A., Daniels, L.M., Dunbar, K.R., Murillo, C.A., and Pascual, I. (2000) *Inorg. Chem.*, **39**, 748.
89. Berry, J.F., Cotton, F.A., Lu, T., Murillo, C.A., Roberts, B.K., and Wang, X. (2004) *J. Am. Chem. Soc.*, **126**, 7082.
90. Lin, S.-Y., Chen, I.-W., Chen, C.-H., Hsieh, M.-H., Yeh, C.-Y., Lin, T.-W., Chen, Y.-H., and Peng, S.-M. (2004) *J. Phys. Chem. B*, **108**, 959.
91. Mohan, P.J., Georgiev, V.P., and McGrady, J.E. (2012) *Chem. Sci.*, **3**, 1319.
92. Georgiev, V.P. and McGrady, J.E. (2011) *J. Am. Chem. Soc.*, **132**, 12590.
93. (a) Chen, I.-W.P., Fu, M.-D., Tseng, W.-H., You, J.-Y., Wu, S.-H., Ku, C.-J., Chen, C.-H., and Peng, S.-M. (2006) *Angew. Chem. Int. Ed.*, **45**, 5814; (b) Shin, K.-N., Huang, M.-J., Lu, H.-G., Fu, M.-D., Kuo, C.-K., Huang, G.-C., Lee, G.-H., Chen, C.-H., and Peng, S.-M. (2010) *Chem. Commun.*, **46**, 1338.
94. Georgiev, V.P. and McGrady, J.E. (2011) *J. Am. Chem. Soc.*, **133**, 12590.
95. Cotton, F.A. and Ucko, D.A. (1972) *Inorg. Chim. Acta*, **6**, 161.
96. (a) Brosset, C. (1935) *Nature*, **135**, 874; (b) Dunbar, K.R. and Pence, L.E. (1991) *Acta Crystallogr.*, **C47**, 23; (c) Watson, W.H. Jr., and Waser, J. (1958) *Acta Crystallogr.*, **11**, 689.
97. Summerville, R.H. and Hoffmann, R. (1979) *J. Am. Chem. Soc.*, **101**, 3821.
98. Bursten, B.E., Cotton, F.A., and Fang, A. (1983) *Inorg. Chem.*, **22**, 2127.
99. Ginsberg, A. (1980) *J. Am. Chem. Soc.*, **102**, 111.
100. Darriet, J. (1981) *Rev. Chim. Miner.*, **18**, 27.
101. (a) Saillant, R. and Wentworth, R.A.D. (1968) *Inorg. Chem.*, **7**, 1606; (b) Wessel, G.J. and Ijdo, D.J.W. (1957) *Acta Crystallogr.*, **10**, 466; (c) Grey, I.E. and Smith, P.W. (1971) *Aust. J. Chem.*, **24**, 73.
102. Stranger, R., Smith, P.W., and Grey, I.E. (1989) *Inorg. Chem.*, **28**, 1271.
103. Heath, G.A., McGrady, J.E., Raptis, R.G., and Willis, A.C. (1996) *Inorg. Chem.*, **35**, 6838.
104. Cotton, F.A. and Troup, J.M. (1974) *J. Chem. Soc., Dalton Trans.*, 800.
105. Green, J.C., Green, M.L.H., and Parkin, G. (2012) *Chem. Commun.*, **48**, 11481.
106. Bauschlicher, C.W. (1986) *J. Chem. Phys.*, **84**, 872.
107. Bo, C., Sarasa, J.-P., and Poblet, J.-M. (1993) *J. Phys. Chem.*, **97**, 6362.
108. Mealli, C. and Proserpio, D. (1990) *J. Organomet. Chem.*, **386**, 203.
109. Reinhold, J., Kluge, O., and Mealli, C. (2007) *Inorg. Chem.*, **46**, 7142.
110. Ghorokov, L.N., Emelyanov, A.M., and Khodeev, Y.S. (1974) *Teplofiz. Vys. Temp.*, **12**, 1307.
111. Souter, P.F., Kushto, G.P., Andrews, L., and Neurock, M. (1997) *J. Am. Chem. Soc.*, **119**, 1682.
112. Gagliardi, L. and Roos, B.O. (2005) *Nature*, **433**, 848.
113. Cavigliasso, G. and Kaltsoyannis, N. (2006) *Dalton Trans.*, 5476.
114. Wu, X. and Lu, X. (2007) *J. Am. Chem. Soc.*, **129**, 2171.
115. Goldberg, D.E., Harris, D.H., Lappert, M.F. and Thomas, K.M. (1976) *J. Chem. Soc., Chem. Commun.*, 261.
116. Dasent, W.E. (1965) *Non-Existent Compounds – Compounds of Low Stability*, Marcel Dekker, Inc., New York.
117. West, R., Fink, M.J., and Michl, J. (1981) *Science*, **214**, 1343.
118. (a) Goldberg, D.E., Hitchcock, P.B., Lappert, M.F., Thomas, K.M., Thorne, A.J., Fjelberg, T., Haaland, A., and Schilling, B.E. (1986) *J. Chem. Soc. Dalton Trans.*, 2387; (b) Power, P.P. (1998) *Dalton Trans.*, 2939.
119. Stürmann, M., Saak, W., Marsmann, H., and Weidenbruch, M. (1999) *Angew. Chem. Int. Ed.*, **38**, 187.
120. Seidu, I., Seth, M., and Ziegler, T. (2013) *Inorg. Chem.*, **52**, 8378.
121. Kurlancheek, W., Jung, Y., and Head-Gordon, M. (2008) *Dalton Trans.*, **4428**.